Hydrogen (deuterium) retention and desorption from boron: Efficient dissociation of molecular hydrogen and absence of diborane desorption

A Afonin, T Cornelius, C Martin, M Minissale, C Pardanaud, P Rial Plaza, E Salomon, T Angot, R Bisson

Nuclear Materials and Energy 47 (2026) 102112

Contents lists available at ScienceDirect

Nuclear Materials and Energy

journal homepage: www.elsevier.com/locate/nme

Hydrogen (deuterium) retention and desorption from boron: Efficient dissociation of molecular hydrogen and absence of diborane desorption ☆

A. Afonin [a,*], T. Cornelius [b], C. Martin [a], M. Minissale [a], C. Pardanaud [a], P. Rial Plaza [a], E. Salomon [a], T. Angot [a], R. Bisson [a]

[a] Aix-Marseille University, CNRS, PIIM, UMR 7345, Marseille, France
[b] Aix-Marseille University, University of Toulon, CNRS, IM2NP, UMR 7334, Marseille, France

ARTICLE INFO

Keywords:
Hydrogen retention
Fusion
Plasma-facing materials
Boronization

ABSTRACT

Understanding hydrogen isotope retention in plasma-facing materials is essential for the safe and efficient operation of fusion reactors. This study investigates hydrogen and deuterium interactions with polycrystalline β-phase boron with surface carbon contamination. Using a combination of X-ray photoelectron spectroscopy (XPS), Scanning electron microscopy (SEM)/Energy-dispersive X-ray spectroscopy (EDX), X-ray diffraction (XRD), Raman spectroscopy, and Temperature Programmed Desorption (TPD), we characterize materials and evaluate the retention, desorption, and possible reaction pathways of hydrogen isotopes. Our experiments demonstrate efficient molecular hydrogen dissociation on boron surfaces and significant isotope retention, even after neutral molecular exposure at room temperature. Importantly, diborane (B_2H_6) production was found to be negligible under available experimental conditions. TPD spectra reveal two distinct desorption features: a low-temperature desorption peak consistent with previous literature and a previously unreported high-temperature desorption peak above 1000 K. We show that repeated thermal cycling enhances boron chemical activity, likely due to boron sublimation and the formation of new active sites. Preliminary experiments suggest that both low-energy and high-energy trapping sites may be accessed through molecular isotope exposure, but without clear evidence of isotope exchange between these sites, and without significantly reducing the population of the initially present isotope. These findings highlight the critical role of boron surface chemistry in hydrogen isotope retention, with potential challenges for tritium management in future fusion devices.

1. Introduction

The limit on the amount of tritium (T) trapped in fusion reactors, imposed by nuclear safety regulations, as well as the necessity to determine the requirements for plasma detachment from the divertor, make fuel recycling one of the important topics in plasma-material studies for deuterium–tritium (D–T) fusion plasma reactors. Following the ITER decision to transition from a beryllium first wall to pure tungsten (W), wall conditioning is necessary in order to decrease impurity influx into the plasma. The first phase of the WEST full W tokamak operation has shown that boronization was a necessary wall conditioning technique to get satisfactory W first wall conditions [1]. Boronization stands out as a highly effective technique due to its oxygen-scavenging capabilities. However, while hydrogen isotopes (HI) have an extremely low solubility in W [2], making it an attractive material for the first wall and other plasma-facing components, introducing additional impurities such as boron (B) may change the characteristics of hydrogen retention in plasma-facing components.

Boronization was extensively researched during the experimental campaign on JET with a carbon wall, which was initially planned for ITER. Studies on amorphous boron films [3–5], as well as on boron carbide [6,7] have shown that boron plays a major role in hydrogen retention. Alimov et al. [6] have conducted a study exposing sintered boron carbide samples to D_2^+ plasma (dominated by D_2^+ ions) with an ion energy of 200 eV/D and a flux of $\sim 10^{21}$ D^+ m^{-2} s^{-1} for a total fluence of 2×10^{24} D^+ m^{-2}. They have shown that D atoms diffuse into the bulk at temperatures above 553 K and accumulate up to a maximum concentration of about 0.2 at.%. Additionally, increasing exposure temperature led to an increase in the amount of D retained in B_4C: from 4×10^{20} D m^{-2} at 550 K to $>2 \times 10^{21}$ D·m^{-2} at 923 K. A study by Yamauchi et al. [7], where a 0.1 mm B_4C layer was deposited on a graphite substrate using chemical vapor reaction and

☆ This article is part of a Special issue entitled: 'PFMC-20' published in Nuclear Materials and Energy.

* Corresponding author.
E-mail address: aleksandr.afonin@univ-amu.fr (A. Afonin).

https://doi.org/10.1016/j.nme.2026.102112
Received 1 July 2025; Received in revised form 6 March 2026; Accepted 30 March 2026
Available online 31 March 2026

then irradiated by 1.7 keV H ions with a flux of 1×10^{19} H^+ m^{-2} s^{-1} and average fluence of 5×10^{22} H^+ m^{-2}, has shown that the total amount of retained hydrogen at room temperature was 1×10^{22} H m^{-2}. Temperature Programmed Desorption (TPD) evidenced a small production of methane (CH_4) concurrent with H_2 desorption, with a CH_4 to H_2 ratio on the order of 0.03. After withdrawing carbon for the ITER design due to retention concerns, the primary materials for the first wall and the divertor were only beryllium and W and boronization was not considered anymore, since beryllium has high oxygen gettering properties. However, the recent full-W design of ITER reintroduces boronization as a wall conditioning technique, which highlights the scarcity of the literature on hydrogen–boron interactions beyond boron carbide materials.

There are several studies on HI thermal desorption from amorphous boron which report HI desorption in the range of 300–1000 K, with two desorption peaks located around 500 K and 700 K, after exposure of boron powder to hydrogen atmosphere [3,4], as well as after the ion irradiation [8,9]. Additionally, a recent work of Abe et al. [10] has shown the retention of D_2 neutral gas on boron amorphous/crystalline powder with two desorption peaks at similar temperatures. To the best of our knowledge, the only experimental hydrogen isotope ion retention study on polycrystalline boron to date were realized by Kodama et al. [11] and by Oya et al. [5]. Using an ion fluence of 5×10^{21} D^+ m^{-2} at various implantation temperatures, ranging from 304 to 573 K, they have shown that polycrystalline boron retains up to 100% of implanted deuterium ions at room temperature. Retention decreased to 35% when the sample was implanted at 573 K. This behavior was explained by the TPD observation of a large HI desorption range (300–1000 K) with two desorption peaks located around 500 K and 700 K, similar to amorphous boron results. The term "pure boron" is avoided throughout this work as well as for the referenced literature, since elemental analysis consistently reveals non-negligible surface contamination [5,8,10,11]. In the literature, surface sensitive analysis like X-ray photoelectron spectroscopy (XPS) and Auger electron spectroscopy have measured boron purity varying from 94 at.% B to 62 at.% B with surface contaminants being oxygen (from 2 at.% O to 22 at.% O) and carbon (from 3 at.% C to 12 at.% C). Nevertheless, Abe et al. [10] reported Energy-dispersive X-ray spectroscopy (EDX) measurements of their boron powder yielding a mean composition (within 200 nm below the surface) of 94 at.% B, 2 at.% O and 4 at.% C, despite their XPS measurements indicating 62 at.% B, 22 at.% O and 12 at.% C. Thus, carbon and oxygen contaminations are located mainly within the first nanometers of the surface. To summarize the experimental literature, several groups reported that boron exhibits significant HI retention with two desorption peaks located around 500 K and 700 K, independently of the microstructure (amorphous or polycrystalline) and the variation of near-surface contamination up to 30 at.% of carbon and/or oxygen. We would like to stress that the base pressure designed in ITER will be at best in the 10^{-7} Pa range [12], i.e. the base pressure of our experimental setups. It is well known in surface science that most materials introduced into an ultra-high vacuum environment present surface contamination by carbon and oxygen at the level of tens of atomic percent [13], even after baking at several hundred kelvin. Thus, the present study and the given literature survey is relevant to ITER's expected vacuum conditions. From the modeling side, a numerical study of crystalline α-boron by Wagner et al. [14] showed that implanted H is mobile at room temperature and should create interstitial molecular H_2. It was estimated that H_2 should diffuse towards the surface only at high temperatures, where it will desorb through an intermediary dissociation step. This result is consistent with the computational work of Mårlid et al. [15] where it was determined that α-boron should adsorb H_2 molecules through a dissociative chemisorption, i.e., hydrogen isotopes are expected to be present as adsorbed atoms at the surface of α-boron. The activation energy for H_2 diffusion was evaluated to be ~2.2 eV, which should be consistent with the experimental observation of Oya et al. Even though α-boron is not thermodynamically stable and should transition to β-boron, these calculations can give some insight into β-boron behavior, which is difficult to address computationally because of its large supercell. Recently, a recent experimental-modeling study by Hiroto et al. [16] showed that β-boron thermal annealing with a H_2 flow above 700 K can lead to an abrupt lattice expansion, which is supposedly due to the formation of the sub-hydride (H_xB_{105}). However, there was no measurement of H_2 retention or desorption to confirm this interpretation, and the possibility of molecular H_2 absorption in β-boron remains to be demonstrated.

Finally, as diborane (B_2H_6/B_2D_6) is a highly toxic gas, it is important to assess whether it can be produced during thermal annealing of hydrogen-implanted boron.

This work aims to answer several open questions about the behavior of boron with respect to hydrogen isotopes. In particular, is diborane (B_2H_6) desorption concurrent with the desorption of H_2? Can hydrogen isotopes be retained significantly above 900 K on boron, and if so, what are the processes responsible for this retention? Can molecular hydrogen dissociate on boron surfaces and under what conditions? And finally, could isotopic exchange be used to decrease tritium inventory in boron-coated plasma-facing components?

Table 2.1
Impurities reported by the manufacturer using inductively coupled plasma mass spectrometry on the 99.9 wt% polycrystalline powder used for the production of sintered boron samples.

Element	ppm	Element	ppm	Element	ppm	Element	ppm
Ag	50	**Al**	20	**As**	10	**Cd**	10
Co	20	**Cr**	50	**Cu**	10	**Fe**	20
Mg	10	**Pb**	40	**Si**	20	**Sn**	70
Ti	20	**Zn**	50				

2. Materials and methods

Boron samples, which were made of a 99.9 wt% polycrystalline boron powder, sintered into rectangular prisms (10 × 10 × 1 mm in size) were purchased from Neyco and were characterized in two separate ultra-high vacuum (UHV) setups at the PIIM laboratory (Aix-Marseille University) as well as on benchtop instruments.

Results of the inductively coupled plasma mass spectrometry analysis performed on the boron powder by the manufacturer is presented in Table 2.1. The boron powder had small amounts (in the 10–70 ppm range) of mostly metallic impurities, which are likely insignificant for the following hydrogen isotope retention measurements.

Two samples from the same fabrication batch were characterized in the XPS chamber prior to and after D_2^+ ion implantation and annealing. One of the two samples was further characterized *ex situ*, chemically using EDX, and structurally using scanning electron microscopy (SEM), confocal laser scanning microscopy (CLSM), Raman spectroscopy, and X-ray diffraction (XRD). Additionally, the third sample was characterized by CLSM and SEM after the implantation/TDS experimental campaign.

The first experimental setup was used for XPS. Its schematics are presented in Fig. 2.1. It is equipped with a non-monochromatic Mg Kα radiation source ($h\nu$ = 1253.6 eV) from an X-ray tube from PREVAC [17]. The emitted photoelectrons were detected with an R3000 analyzer from Scienta Omicron, equipped with a microchannel plate detector. The spectral resolution, determined from the full width at half maximum (FWHM) of the Ag 3d core levels measured on a clean Ag surface, was 1.1 eV. All spectra are referenced to the substrate Fermi level. Deuterium was implanted into the sample using a PREVAC IS 40C1 ion source near room temperature [in the range 298–315 K, so-called NRT in the remainder of the text]. The majority ion species (>95%) is D_2^+, as verified with a quadrupole mass filter analyzer (Hiden EQP), and they are accelerated to a kinetic energy of 500

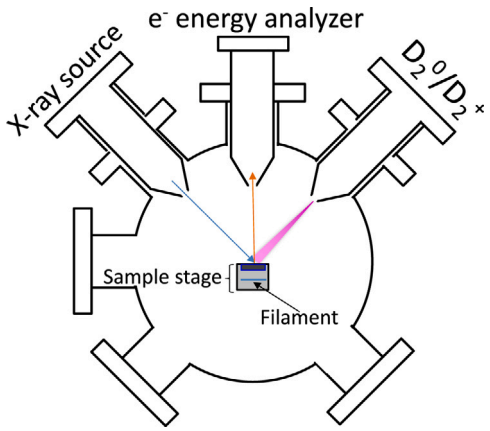

Fig. 2.1. Schematic representation of the XPS setup. The rod fixing the sample stage to the chamber is positioned directly behind the stage in this projection.

eV, i.e., 250 eV/D, and a typical flux of 9.3×10^{15} D^+ m^{-2} s^{-1} was used. The current of the ion flux through the sample stage was measured using a KEITHLEY 616 picoammeter. Knowing the surface of the exposed part of the sample and the surface of the sample stage, the flux can be estimated. Prior to and after deuterium ion exposure, samples were annealed at ~1123 K using a W filament located on the sample stage ~5 mm below the sample. The temperature of the sample is derived from the previously made calibration, where a dummy W-sample with a spot-welded thermocouple was placed into the setup. Then, a constant power input was applied to the filament, and once the sample had reached thermal equilibrium, the relation of chosen power to recorded temperature was recorded.

The second setup was used for hydrogen isotope retention and desorption analysis with *in situ* Temperature Programmed Desorption (TPD), prior to and after ion irradiation/molecular exposure (Fig. 2.2). The experimental setup is thoroughly described in the work of Bisson et al. [18]. The sample is introduced into the vacuum via a motorized rod, where it is pushed through two vacuum stages, which allows for maintaining the UHV condition of the setup (base pressure $< 2.3 \times 10^{-7}$ Pa). Once in the vacuum, the sample is picked up by the transfer rod, which is then used to install the sample into the oven. The oven consists of a molybdenum (Mo) box with the brackets on top to hold the sample and a UHV-compatible W filament on the bottom. The filament is held in place by Mo screws, isolated from the rest of the oven by ceramic rings. The distance between the back of the sample and the filament is ~5 mm. The assembly is fixed to the stainless steel shaft. The temperature of the oven is monitored via a type-K thermocouple located 2 mm away from the sample holder. Since the thermocouple is not directly attached to the sample, its actual temperature is derived from the temperature of the oven using a calibration curve obtained via a dummy W sample with a spot-welded type-K thermocouple. Because the thickness and the thermal conductivity of the W and B samples are different, we checked the thermocouple calibration using two single-color pyrometers (SensorTherm, Metis). We found that the thermocouple calibration and the pyrometer measurements agree once the scarce data on Boron emissivity is taken into account. To give an example, a 1200 K thermocouple measurement corresponds to the temperature range 1020–1220 K from the pyrometer measurement (boron emissivity range 0.4–0.8 in our infrared domain). The output of the thermocouple is connected to a PID controller, which allows to use of the temperature reading to control the power output of the filament power supply, which in turn allows performing consistent linear ramps with a desired rate of temperature increase. Before the irradiations/exposures experimental campaign, the sample was subjected to a degassing procedure consisting of five linear temperature ramps of 1 $K{\cdot}s^{-1}$ up to 1350 K. This allowed us to remove most of the impurities adsorbed onto the surface of the sample; previous works [18,19] have shown that the "cleaning procedure" results in reproducible D retention measurements on W and WO_3 samples, which were extensively researched in this setup. H_2^+ (in the case of diborane production evaluation) or D_2^+ ions were implanted into the sample at NRT using an Omicron ISE 10 sputter ion source with the typical flux of 2.5×10^{16} D^+ m^{-2} s^{-1}. The H_2^+/ D_2^+ ions (majority ion species > 95%) were irradiated only at the sample, which was previously confirmed by the ion-induced luminescence of a quartz sample, recorded by a CMOS camera [18]. The kinetic energy of the ions was set to 250 eV/nucleus. Exposure of boron to H_2/D_2 molecules was performed using the leak valve of the ion gun with the ion gun turned off. After the ion irradiation or molecular exposure, the sample was removed from the oven, while a temperature ramp was performed on the empty oven to remove any H/D adsorbed onto it. The time interval between the end of hydrogen irradiation/exposure and the following TPD measurement was 2.5 h, with the sample kept in UHV at room temperature. The TPD ramp was set at 1 $K{\cdot}s^{-1}$, and the maximum temperature was 1350 K. Desorption of hydrogen isotopes, water isotopologues, and potential diborane isotopologues, as well as potential diborane ion fragments, was measured by a quadrupole mass spectrometer (QMS HIDEN Analytical HAL 301), which is differentially pumped and located in the line-of-sight of the sample. The line-of-sight geometry allowed us to detect and quantify the desorption of sticky molecules (like water and diborane) during the TPD. Hydrogen isotope retention was calibrated with hydrogen isotope leaks [20]. D retention was quantified from the TPD spectra of all deuterium-containing species: HD (because of constant presence of H_2 contamination in the vacuum chamber), D_2, HDO, and D_2O (given the O contamination of the sample surface), which correspond to m/z = 3, 4, 19, and 20, respectively [21]. Boron hydride masses were not followed in the retention study (Section 3.3) since they have not been registered during the measurements of the diborane ionization fragments (Section 3.2). To address the background contribution, the subtraction is performed by extrapolating the background signal before and after the TDS ramp onto the rest of the spectrum. Then, the extrapolated background signal is subtracted from the raw data. In some cases, such as with a D_2 desorption, the background signal can be fitted with a linear function; in others, for example, with water isotopologues, the background must be fitted with a polynomial. Because the background signal, especially for heavy water, changes its behavior from one experiment to another, it is not possible to automatically pretreat the data. Instead, each TDS spectrum must be reviewed independently.

3. Results and discussion

3.1. Sample surface characterization

SEM shows an irregular polycrystalline structure with a typical grain size of ~10–50 microns (Fig. 3.1). EDX analysis, with an interaction depth in the order of ~1 μm, shows a composition of 92.0 at.% B, <0.5 at.% O, and 7.6 at.% C.

The crystal structure of the sample was characterized by X-ray diffraction using a four-circle X'Pert Pro MRD diffractometer from Panalytical equipped with a Cu anode (λ = 1.54 Å). Fig. 3.2(a) presents the X-ray diffractogram recorded on the present sample. The measured 2-θ positions of the diffraction signals are in very good agreement with those expected for β-phase boron as reported by Slack et al. [22]. The intensities of the Bragg peaks differ from [22], which may be due to slight preferred crystalline orientations of the present sample.

Raman spectra were obtained using a Horiba Jobin Yvon HR800 with excitation wavelengths of λ_L = 633 nm, a 100× objective lens (numerical aperture of 0.9), and a 600 grooves/mm grating. The resolution was about 1 cm^{-1}. Power was kept at 1 mW μm^{-2} to prevent laser damage, but tests were done from 0.01 to 10 mW μm^{-2} without noticeable change of the sample surface. Expanding the sampling area

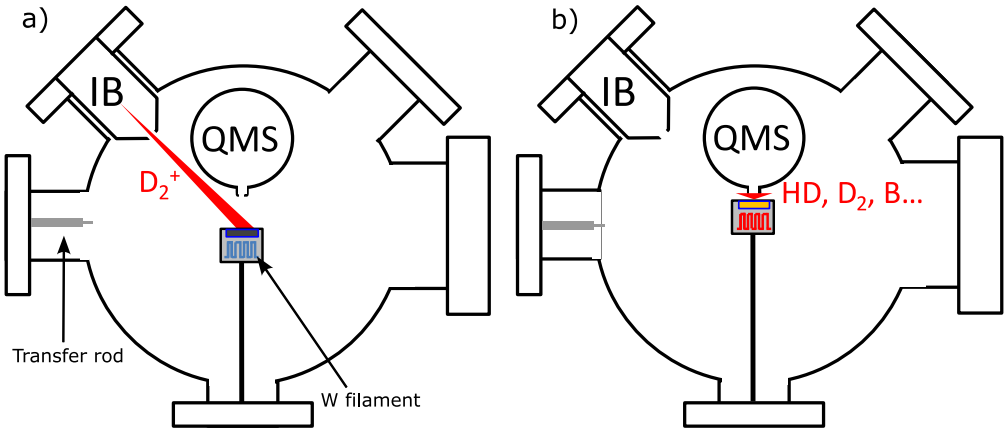

Fig. 2.2. Schematics of the implantation/TPD vacuum setup during (a) irradiation of the sample surface with D_2^+ using a sputter ion source (IB), (b) temperature programmed desorption measurement, where species from the surface are collected by a mass spectrometer (QMS).

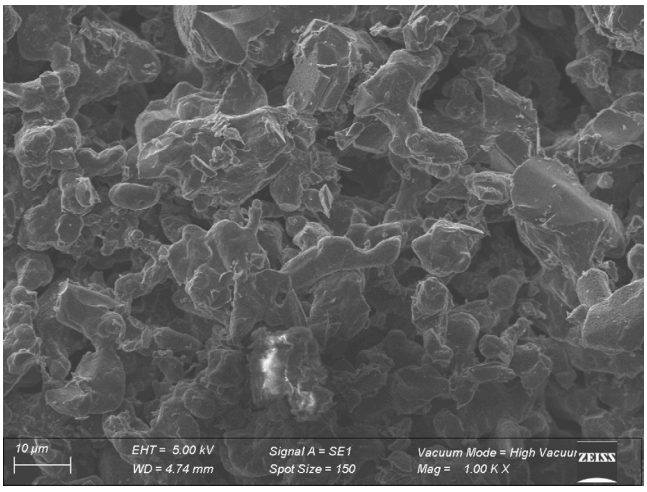

Fig. 3.1. Scanning electron microscopy (SEM) image of the boron sample surface.

did not alter the relative intensities of the Raman peaks, confirming the homogeneity of the surface. This suggests that the recorded spectra represent an average over multiple crystallographic orientations within the laser-excited volume. Consequently, the individual crystallite size must be significantly smaller than 1 µm. The measured spectra, shown in Fig. 3.2(b), differ from those of the $\alpha-$ and $\gamma-$ phases but are comparable to Raman measurements of the β-phase boron [23–25]. Small variations are observed in the literature from one reference to another. These differences may result from local disorder, which affects symmetry and bond lengths, and consequently alters band intensities and positions.

3.1.1. XPS analysis

To analyze the near-surface layer elemental composition of samples (several nm of interaction depth), XPS measurements in the B1s, C1s, and O1s core levels were carried out on two samples from the same batch. Ion implantation and molecular exposure were carried out *in situ* to prevent air exposure of the sample.

Fig. 3.3 presents XPS spectra of the first pristine boron sample, where carbon and oxygen contamination were found. The peak maxima for B1s, O1s, and C1s spectra were 187.3 eV, 532.1 eV, and 281.8 eV, respectively. Quantification of near-surface contamination is performed by comparing the area under the B1s, O1s, and C1s peaks using the equation: $n_x = \frac{I_x/S_x}{\sum I_i/S_i} \times 100\%$, where n_x is the element x ratio, I_i and S_i are the peak integral intensity and sensitivity factor [26,27] defined by the photoionization cross-section of element *i*, respectively.

XPS near-surface composition is found to be 79.9 ± 0.1 at.% B, 9.1 ± 0.1 at.% O, and 11.0 ± 0.1 at.% C for the first pristine boron sample. The second pristine boron sample yields a near-surface composition of 66.5 ± 0.2 at.% B, 11.4 ± 0.1 at.% O, and 22.1 ± 0.2 at.% C. Thus, strong surface contamination is present at the XPS interaction depth (~1 nm) of 99.9 wt% pure boron, even after ~1123 K annealing in UHV.

Then, the two boron samples were irradiated with an ion fluence of ~1.67×10^{19} D^+ m^{-2} at NRT, which was found sufficient for the XPS surface shifts to reach a stable value, yielding repeatable results.

Before discussing the effect of ion exposure, it is worth noting that the B1s, O1s, and C1s spectra can be further decomposed into several sub-peaks, which are commonly attributed in the literature to different bonding environments. However, the deconvolution of boron-related spectra is challenging, since the degree of consensus regarding the exact assignment of the sub-peaks is limited. In this work, the analysis is therefore restricted to a qualitative discussion of the variations in the relative intensity of the sub-peaks, i.e., in the overall peak shape evolution. The deconvolution was performed using Voigt profiles (Lorentzian 20% and Gaussian 80%) on a Shirley background. Exposing the first sample to D_2^+ ions led to a shift of the B1s and O1s binding energy peaks by +1.2 eV, with a conservation of the ratio of the sub-peaks. However, the C1s spectrum shifted by +1.7 eV, with a change of sub-peaks relative intensity (Fig. 3.4). After annealing the sample to 1123 K, the XPS peaks shifted back towards the pristine position; however, not completely. The B1s and O1s spectra have shifted back by −0.4 eV, while the C1s peak has shifted back by −0.68 eV, restoring the initial sub-peak ratio. The shifts in the core levels after the irradiation and annealing are related to a modification in the sample's electrical conductivity, which depends on the amount of carbon, as described by Slack et al. [22]. While an accurate analysis of the sample composition is beyond the scope of this work, Fig. 3.4 clearly shows that the C(C-B) component at ~282 eV decreases after irradiation and increases after annealing, which justifies the observed behavior: shifting to a lower binding energy due to increased conductivity of the sample.

Exposing the second boron sample to D_2^+ ions for the same fluence led to a shift of both B1s and O1s peaks by +0.4 eV (from 187.4 to 187.8 eV and from 532.0 eV to 532.45 eV for B1s and O1s, respectively), with a conservation of the ratio of the sub-peaks. Interestingly, the C1s peak has not shown any meaningful shift (Fig. 3.5). It must also be noted that the relative amount of carbon in the near-surface layer has noticeably decreased after D ion implantation and 1123 K annealing: the surface composition of the second boron sample became 71.8 ± 0.2 at.% B, 10.3 ± 0.1 at.% O, and 17.9 ± 0.2 at.% C.

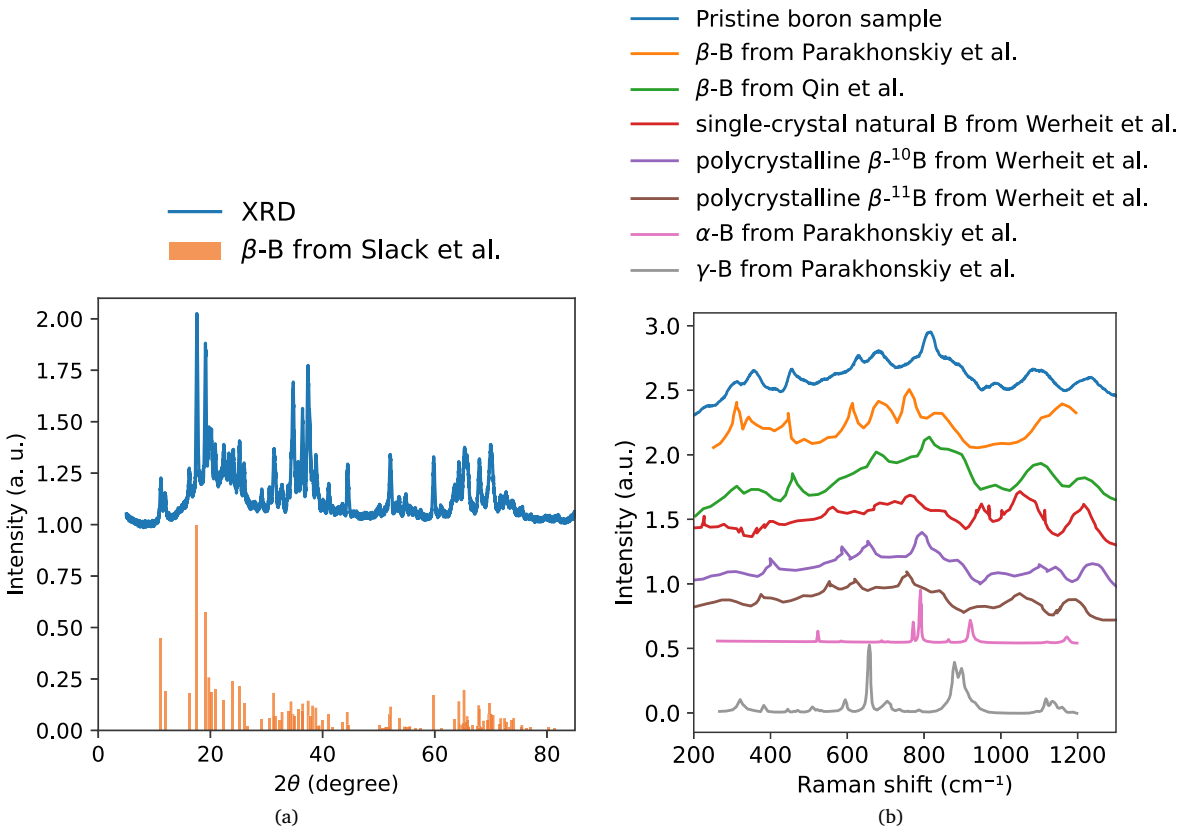

Fig. 3.2. (a) Comparison of the obtained XRD spectrum with the reference spectrum measured on the single-crystal β-phase B by Slack et al. [22]. (b) Comparison of the measured Raman spectrum with the measurement performed on the polycrystalline β-phase boron from [23–25], as well as the single-crystal B from [25] and α-phase B and γ-phase B from [23].

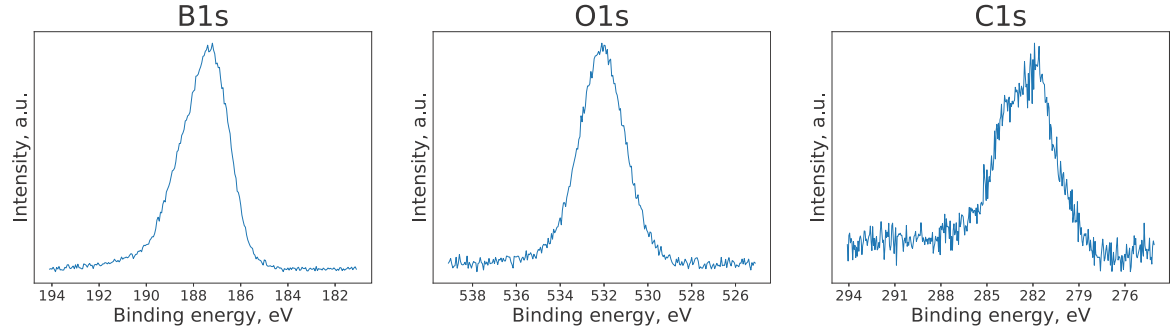

Fig. 3.3. Measured XPS spectra of the first pristine boron sample.

Finally, exposing the boron samples to a similar amount of molecular D_2 at room temperature (~$3.8 \cdot 10^{-4}$ Pa for 30 min or ~0.7 Pa·s) yielded no change in the XPS spectra.

3.1.2. Discussion on the structural and chemical properties of boron samples

XRD, Raman, and SEM measurements had consistently characterized the boron samples of this study as β-phase polycrystalline materials. The boron sample, being 99.9 wt% pure in the bulk nevertheless presented an inhomogeneous level of contamination, which increases as one uses surface-sensitive techniques. Comparison of XPS and EDX measurements indicates that oxygen impurities are only located within a nanometer of the surface, while carbon impurities may be present to the 8 at.% level at the micron range from the surface.

It is worth noting that the XPS measurements did not produce repeatable results upon deuterium ion implantation for the two samples of this study, even though they were from the same batch. A similar inconsistent behavior was already observed by Okuno and coworkers: an absence of B1s XPS shift upon D ion implantation was mentioned in the boron polycrystal of Kodama et al. [11], while a shift of around +0.3 eV was observed in the polycrystal studied by Oya et al. [5]. Okuno and coworkers used boron samples with varying carbon content on the surface, from 3 at.% to 12 at.%. Given that the polycrystalline boron samples used in the present study also have different amounts of carbon on the surface and present different B1s XPS shifts upon D ion implantation, we propose that the difference in B1s XPS shift could be related to the C content of boron. The rigid shifts of both B1s and O1s could indicate the charging of the surface by D_2^+ ions due to the high electrical resistivity of boron, indeed, and one must stress that the electrical conductivity of boron greatly depends on the carbon content, as shown by Slack et al. [22]. Even a variation within 1 at.% of C

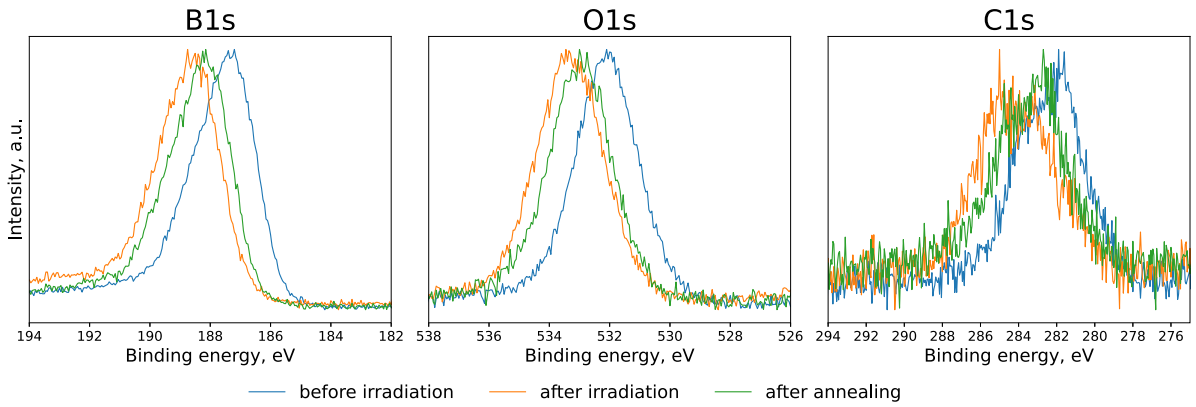

Fig. 3.4. Comparison of normalized B1s, C1s, and O1s XPS spectra before, after D_2^+ irradiation, and after subsequent annealing for the first boron sample (11% C surface impurity).

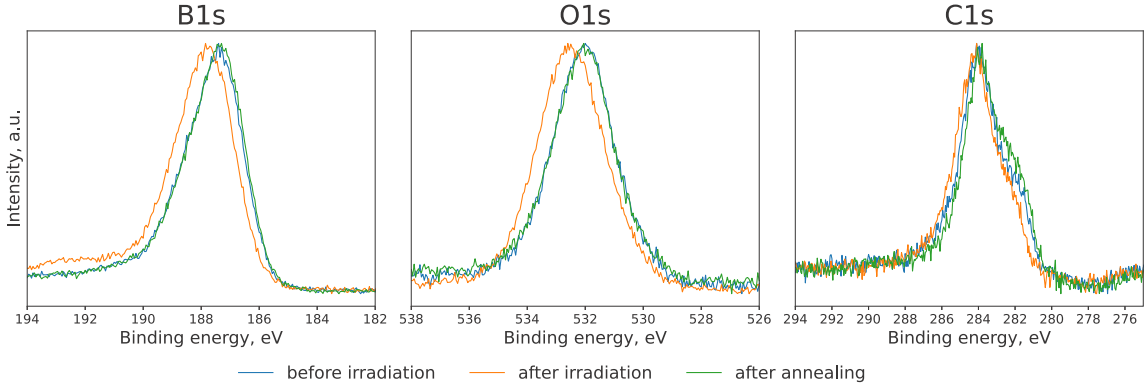

Fig. 3.5. Comparison of normalized B1s, C1s and O1s XPS spectra before, after D_2^+ irradiation and after the following annealing for the second boron sample (22% C surface impurity).

content has led to orders of magnitude of conductivity increase in the single crystal samples, which were studied in the work of Slack et al. Thus, the difference in rigid shift of B1s and O1s in our two boron samples could be explained by a different extent of charging upon D_2^+ ion implantation related to their difference in near-surface carbon concentration. Additionally, the decrease in binding energy after the annealing could be explained by the increased electrical conductivity of B at higher temperatures, leading to the removal of the electrical charge. Furthermore, an additional chemical effect could be at play, as we observed a difference in the C1s shape for the two samples, as well as different shift patterns upon D_2^+ ion implantation. Considering the complexity of the XPS behavior of polycrystalline boron observed in the present study and in the studies of Okuno and coworkers, systematic work on the origin of the B1s XPS shift should be undertaken in the future.

3.2. Evaluation of diborane production during temperature annealing

Diborane production from boron implanted with hydrogen isotopes was evaluated during TPD measurements. The partial ionization cross sections of diborane parent and fragment ions are well known for a large range of electron impact energies [28] and are used to identify and quantify whether diborane desorption is concurrent with H_2/D_2 desorption as detected by electron ionization mass spectrometry. There are 14 parent and fragment ions from B_2H_6, ranging from m/z = 1 up to m/z = 28. The highest partial cross sections for diborane ions are in the m/z = 20–28 range, where two boron atoms are still present in the fragment. Lighter fragments contain solely one boron atom and have an excess of kinetic energy, which can affect the detection efficiency of mass spectrometers. Therefore, we focused the analysis on the more reliable m/z = 20–28 range, taking into account the known natural abundance of ^{10}B and ^{11}B (19.9% and 80.1% respectively).

Fig. 3.6 presents the raw signal of a TPD measurement realized after an H_2^+ ion implantation with a fluence of 2.5×10^{21} H^+ m^{-2}. The most intense desorption signal comes from m/z = 2 and m/z = 28. The former m/z signal corresponds to H_2^+ in the mass spectrometer, which could originate from the desorption of H_2 and/or the desorption of B_2H_6. The latter m/z signal could correspond to the $B_2H_6^+$ parent ion from diborane desorption and/or CO^+ originating from CO desorption from the hot filaments of the mass spectrometer ionization head and the TPD oven.

In order to identify unambiguously the chemical composition of the desorption flux (H_2, B_2H_6, CO…), we compare in Fig. 3.7 the m/z = 20–28 signals expected after diborane ionization with the TPD measurements obtained at different temperatures. All m/z signals are normalized with respect to m/z = 24, which is the most probable m/z signal expected in the case of diborane ionization.

From Fig. 3.7, it is evident that the desorption flux from the TPD of a hydrogen-implanted boron does not correspond to the one expected from diborane desorption. To estimate an upper limit of the ratio of diborane production to the H_2 desorption, we exploit the cracking pattern at 388 K, assuming that the m/z = 24 signal originates solely from all diborane isotopologues ion fragments (B_2H_2, B_2H_3, B_2H_4, with boron atoms composed of the natural ^{10}B and ^{11}B abundance). In that case, and accounting for the difference in absolute partial cross sections, the ratio of measured B_2H_6 to H_2 (diborane branching ratio) is $<4.8 \times 10^{-3}$. At the highest temperature (1350 K), the same exercise performed without background subtraction gives a branching ratio of $<1.5 \times 10^{-3}$. Repeating the experiments on boron implanted with deuterium ions, we determine that the branching ratio for deuterated

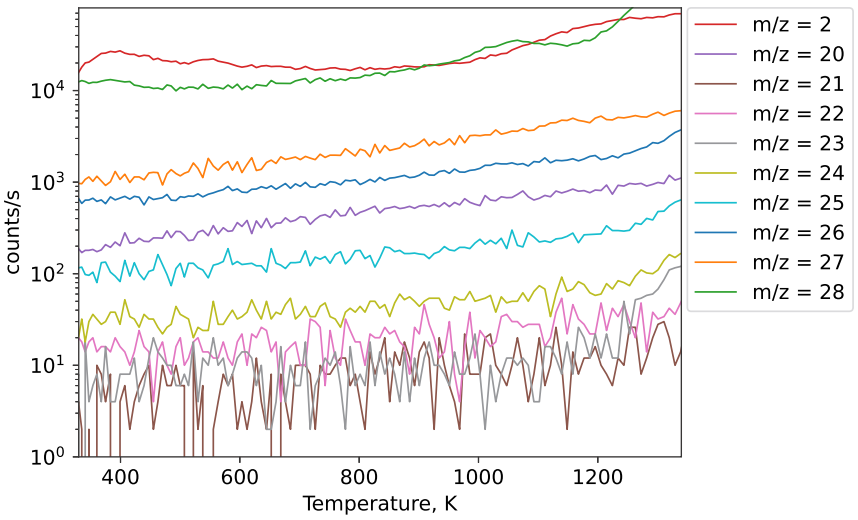

Fig. 3.6. Raw TPD measurement after H_2^+ exposure for potential sources of diborane ion fragments.

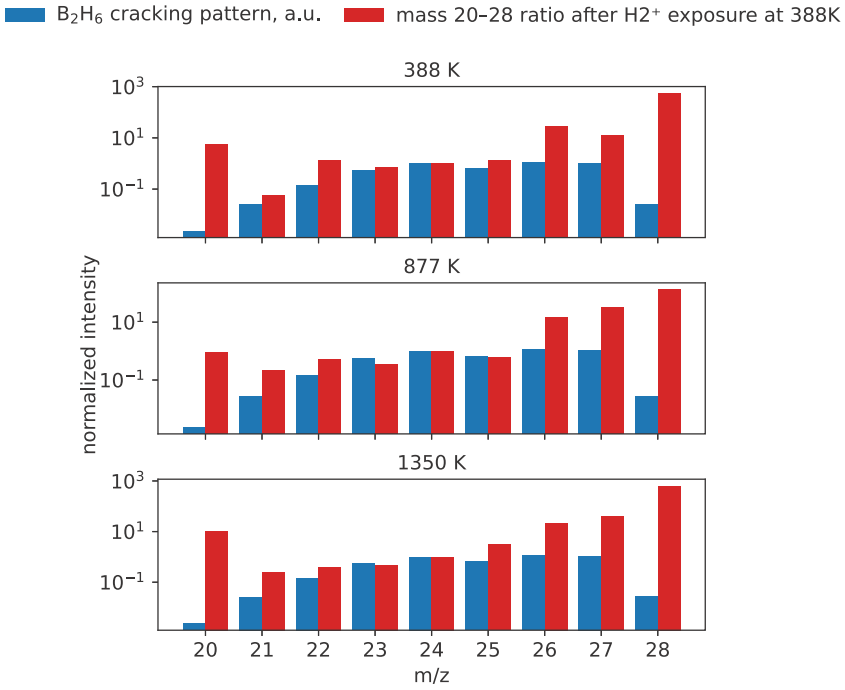

Fig. 3.7. Comparison of diborane cracking pattern with the measured desorption at different temperatures.

diborane (assuming no isotope effect on partial ionization cross sections), the B_2D_6/D_2 branching ratio is $<8.9 \times 10^{-3}$. Therefore, we can conclude that under the present experimental conditions (hydrogen isotope implantation at room temperature with a fluence of $\sim 2.5 \times 10^{21}$ H^+ m^{-2}), diborane production is below detectable limits at desorption temperatures up to 1350 K. Note that in the present work we confirm the absence of boron in the desorption flux below 900 K reported by Abe et al. [10]. Thanks to the detailed study of the cracking pattern, we are in addition able to give an upper limit to diborane emission during thermal cycling of boron.

3.3. Deuterium retention in boron: high desorption temperature and chemical activity towards molecular deuterium

Having demonstrated that diborane production is negligible in our experimental conditions, we turn to the study of deuterium retention in polycrystalline boron sample with C surface contamination. Fig. 3.8 presents a raw TPD measurement obtained after deuterium ion exposure with a fluence of 2.8×10^{19} D^+ m^{-2}.

The TPD spectrum shows two main desorption features. First, a low-temperature broad desorption peak in the 330 K–810 K range, with a desorption flux composed mainly of D_2, HD, HDO, and a small amount of D_2O. This broad desorption peak is comparable to the one observed by Oya et al. on polycrystalline boron [5]. The second desorption peak is located at a much higher temperature (> 1000 K), and the desorption flux is composed primarily of D_2 molecules. The observation of this high-temperature peak is unprecedented, and it appears more intense than the low-temperature desorption peak.

After converting the raw TPD signals into an absolute desorption flux (in D m^{-2} s^{-1}), the estimated deuterium retention is found to be 7×10^{19} D m^{-2}, i.e., more than twice the implanted ion fluence. This surprising result is reproducible and can be easily explained. During the ion implantation, the pressure in the sample chamber rises from 10^{-7} Pa (base pressure) to 10^{-4} Pa (ion gun feed gas pressure).

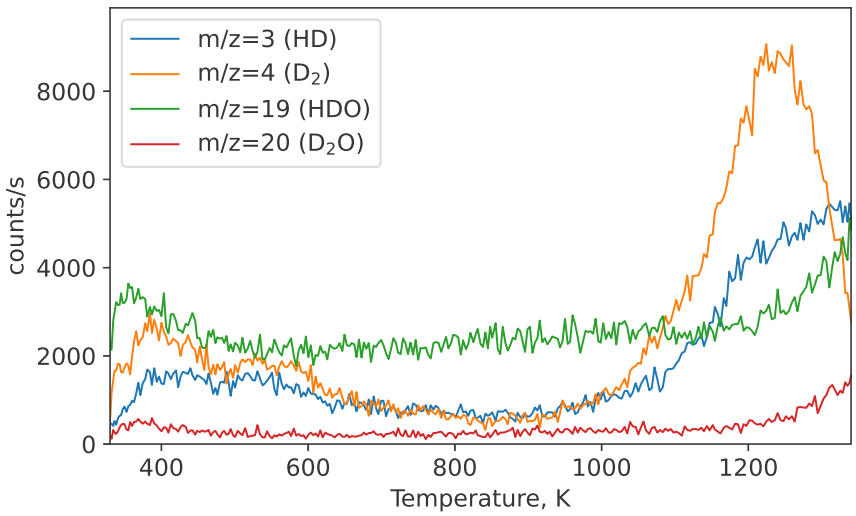

Fig. 3.8. Raw TPD signal for D-containing species (HD, D_2, HDO, and D_2O). Note: the relatively high baseline of the m/z = 19 signal is related to the materials which were used in the ionization stage of the QMS.

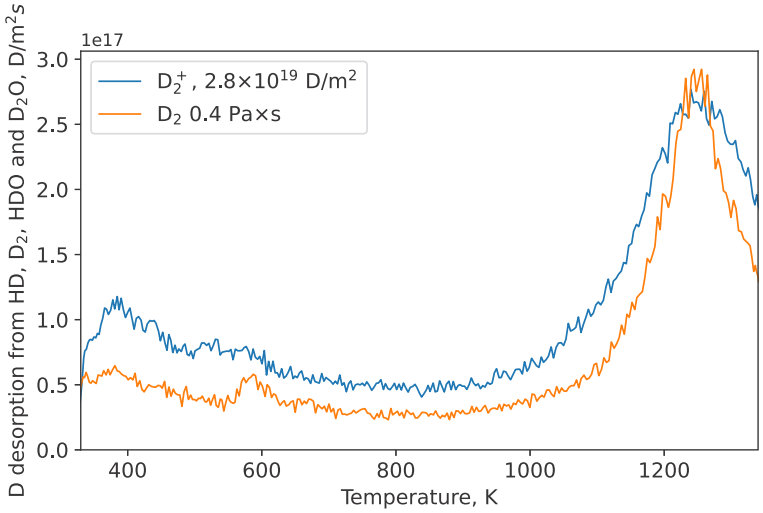

Fig. 3.9. Comparison of D_2 desorption after D_2^+ implantation and D_2 exposure with the same pressure and implantation/exposure duration.

Using the kinetic theory of gases, one can estimate that during D ion implantation, a D_2 molecular exposure of 2×10^{19} D m^{-2} s^{-1} is concurrent with the ion flux of 2.5×10^{16} D^+ m^{-2} s^{-1}. This is usually not a concern with plasma-facing materials like W, where the native oxide makes the surface inactive to molecular dissociation [29]. But the case of deuterium-implanted boron seems different.

In order to verify whether neutral hydrogen isotopes could react with boron, the sample was exposed to D_2 molecules at room temperature at the same pressure and for the same duration as for an ion implantation. Fig. 3.9 shows that the obtained TPD spectra show similar desorption in terms of absolute values as well as peak positions for D_2 exposure and for D_2^+ implantation, suggesting that deuterium is solely adsorbed at the surface during exposure to D_2^+ at NRT.

The observation of significant deuterium retention from exposure to neutral D_2 molecular gas is consistent with the findings of Abe et al. [10], who reported the first observation of D retention from D_2 neutral gas exposure on boron powder. They attributed the D retention to dissociative chemisorption on the boron surface, with two desorption peaks occurring around 500 K and 700 K. This is in good agreement with the low-temperature desorption feature observed in the present study in the 330–810 K range. Notably, Abe et al. attributed the larger D_2 retention on powder compared to boron films to the significantly higher surface area of the powder samples. In the present study, the chemical activity towards molecular D_2 is instead observed on a sintered polycrystalline boron sample, suggesting that the dissociative chemisorption of molecular hydrogen isotopes is not limited to high-surface-area powder morphologies but is also active on bulk polycrystalline boron, albeit enhanced by the presence of active sites created during ion implantation and thermal cycling.

In summary, we demonstrated that an implanted polycrystalline boron sample with C surface contamination was able to retain similarly large quantities of hydrogen isotopes solely with molecular exposure. The origin of the chemical activity of implanted boron needs to be further investigated to be understood. We present in the following some preliminary observations that could guide future studies.

3.4. Exploring the origin of deuterium desorption from boron above 1000 K

Desorption of retained hydrogen isotopes in boron was found to occur through two desorption peaks, the most intense desorption peak being the one above 1000 K. In the course of the experimental campaign, the desorption of D_2 molecules from both peaks was found

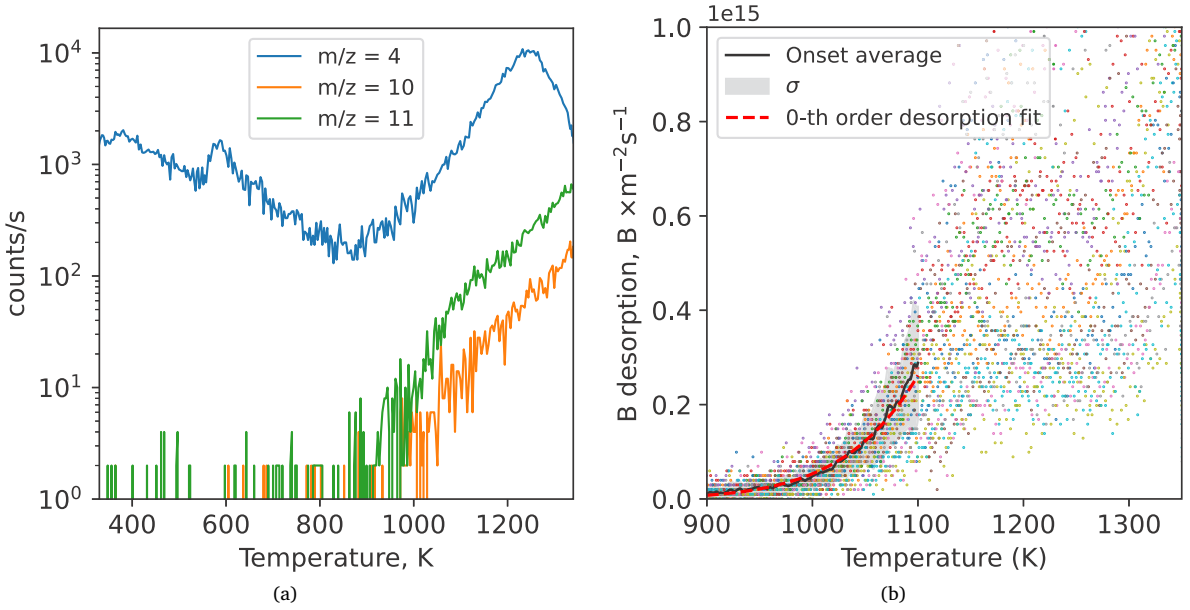

Fig. 3.10. (a) Desorption of D_2,^{10}B and ^{11}B after neutral D_2 exposure. (b) Scatter plot of all recorded boron desorptions, showing the consistent onset.

to increase consistently: after twelve molecular exposure/TPD experiments, the first peak integral increased by a factor of 1.6, while the higher temperature peak increased by a factor of 2.8, with the total desorption increase by a factor of 2.5. Thus, the boron sample seemed to have more and more active sites able to trap D_2 molecules upon repeated molecular exposure/TPD experiments.

The evolution of boron chemical activity may be linked to the following observation made during TPD and presented in Fig. 3.10(a). The high temperature D_2 desorption peak correlates with boron atoms sublimating from the surface. We confirm that it is boron sublimation, indeed, because the ratio of m/z = 11 and m/z = 10 follows the natural abundance of boron isotopes. The total amount of sublimated boron did not saturate over the course of thirty-one exposure/TPD experiments, and the accumulated amount of boron desorbed during the experimental campaign was estimated to be 4×10^{19} m^{-2}.

Fig. 3.10(b) is a scatter plot of the 31 observations of boron sublimation as a function of sample temperature. One can notice that the onset of boron sublimation is consistent both in terms of temperature and absolute values of desorption until ~1100 K. For higher temperatures, the boron sublimation rate is more scattered. Therefore, we use the boron sublimation data below 1100 K to estimate boron sublimation energetics. We assume that the observed sublimation is an equilibrium between the dense boron material and the dilute sublimated boron in the gas phase. Given that our TPD measurements were performed at 1 $K{\cdot}s^{-1}$, we can consider a quasi-equilibrium condition, and one can approach the initial exponential rise of sublimation as zeroth-order desorption with a simple form of the Arrhenius equation $v \times \exp(-E_a/kT)$. Fitting the common rising leading edge of the boron sublimation peak below 1100 K in figure 11b, we determine the activation energy for boron sublimation to be $E_a = 1.51 \pm 0.02$ eV with a prefactor $\nu = 2.17 \times 10^{21} \pm 0.43 \times 10^{21}$ $m^{-2}s^{-1}$.

To summarize, we propose that the sublimation of boron atoms should participate in the creation of active sites at the surface that promote molecular deuterium dissociation and retention. These active sites retain hydrogen isotopes efficiently above 1000 K, i.e., they are high activation energy trapping sites.

3.5. Isotopic exchange in high activation energy trapping sites

The considerable deuterium retention measured in implanted boron and the observed high-temperature desorption peak raise concerns about tritium buildup within boron layers deposited on the first wall of modern fusion reactors. During plasma discharges and wall baking, the ITER's first wall temperature is not going to exceed 1000 K, which may be insufficient to retrieve all hydrogen isotopes retention in boron layers.

Considering the presence of HD signal in the TPD measurements after D_2 exposure (Fig. 3.8), we concluded that hydrogen isotope retention is not occurring in a molecular form; rather, it dissociates at the surface at room temperature and can recombine with dissociated H_2 from the vacuum background. Thus, molecular dissociation on boron active sites may offer a possible solution for tritium removal. Exposing a tritiated boron layer to a molecular deuterium pressure could lead to "isotopic exchange cleaning". To test this hypothesis, the following protocol was tested. First, the sample was exposed to 0.4 Pa·s of H_2 to simulate tritium exposure and retention on boron. Second, a partial TPD ramp on the boron sample up to 810 K was performed to free the low-temperature retention sites. Third, boron was exposed to 0.4 Pa·s of D_2 to populate the low-temperature retention sites with the "cleaning isotope". Finally, a TPD was realized up to 1350 K to evaluate how the retention of hydrogen (tritium proxy) in the high-temperature desorption site was affected by the presence of deuterium in the low-temperature desorption sites.

Fig. 3.11(a) compares the desorption of molecular hydrogen with the partial temperature ramp performed after H_2 exposure (named H_2 exposure) and full-range TPD after D_2 exposure (named D_2 exposure) with the full-range TPD of hydrogen-only reference exposure. Figs. 3.11(b) and 3.11(c) compare the same parts of the experiment with a deuterium-only reference exposure. Overall, the experiment shows a noticeable decrease in H_2 desorption from the high-temperature desorption peak of about 35%. However, an increase of HD in a similar amount was observed above 1000 K. Since an increase of D_2 was also observed, this preliminary isotopic exchange experiment exhibits an overall increase of hydrogen isotopes, implying either that hydrogen saturation was not initially reached or that the number of active sites of boron increased during the partial TPD ramp. Regarding the HD signal observed in the low-temperature peak, its magnitude is comparable to that of the D_2-only reference exposure, suggesting it originates from the residual partial pressure composed of H_2 and H_2O rather than from hydrogen transferred from the high-temperature retention sites. Therefore, no clear evidence of isotope exchange between high-

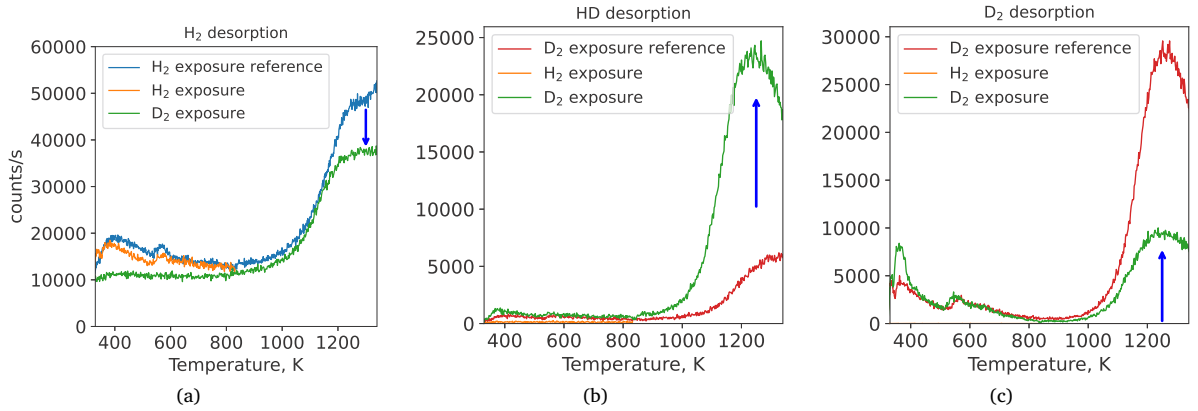

Fig. 3.11. (a) Desorption of H_2 after H_2 only exposure as reference, after H_2 exposure with the partial TPD ramp and after D_2 exposure, showing decrease in H_2 desorption. (b, c) Desorption of HD and D_2 respectively, after D_2 only exposure (as a reference), after H_2 exposure with the partial TPD ramp (signals are close to 0 counts/s) and after D_2 exposure, showing increase in both HD and D_2.

and low-temperature retention sites is observed in this experiment. An improved protocol should be considered in the future and additional studies are required to assess the interaction depth of molecular hydrogen with boron.

4. Conclusions and perspective

Despite working on a bulk high-purity commercial sample, combined XPS, SEM/EDX, XRD, and Raman analyses show the presence of carbon surface contamination at the 10 at.% level in the implantation range of a polycrystalline β-phase boron sample. The presence of surface carbon contamination seems to affect the chemical shift of the B1s peak upon D implantation in the XPS spectra, raising questions about the previous assignment of the B1s shift to the formation of a B–D bond. Subsequent to hydrogen (or deuterium) implantation in boron at room temperature, TPD measurements show that the amount of diborane (or deuterated diborane) is negligible in the desorption flux up to 1350 K.

Desorption of molecular hydrogen isotopes from hydrogen/deuterium ion-implanted boron occurs through two distinct features: a multi-component low-temperature desorption peak between 350 and 800 K and an intense desorption peak above 1000 K. The presently measured desorption below 1000 K is consistent with the work of Kodama et al., Oya et al., Hino et al., and Abe et al. [5,8,10,11], showing a common desorption feature for boron independently of its microstructure (amorphous or polycrystalline, powder or bulk material). However, the intense desorption presented here above 1000 K is unprecedented and was enabled by our TPD setup reaching 1350 K. Quantification of deuterium retention after D_2^+ implantation led to an amount of desorbed deuterium that was higher than the measured ion fluence. Repeating the experiment with D_2 gas exposure only has led to similar TPD and similar retention, evidencing that the vast majority of deuterium retained by the boron sample came from molecular D_2 flux, which were concurrent with (and orders of magnitude higher than) D_2^+ ion flux. Thus, hydrogen isotope ion implantation in sintered polycrystalline boron leads to a material that readily dissociates and retains molecular hydrogen isotopes, similarly to boron powder [10].

We found that repeating D_2 exposure and TPD experiments led to a continuous increase of deuterium retention while boron sublimation was systematically measured during the high-temperature desorption peak of hydrogen isotopes. Boron sublimation during high temperature cycling may be linked to the observed increased chemical activity towards molecular hydrogen isotopes.

Considering the measured important hydrogen isotope retention and the high desorption temperature, we explored an isotopic exchange cleaning protocol to counteract the possible accumulation of tritium in boron layers. Using partial TPD followed by deuterium exposure, a partial decrease in H_2 desorption from the high-temperature retention sites of about 35% was observed, accompanied by an overall increase in total hydrogen isotope retention, consistent with D_2 populating both low- and high-temperature trapping sites. However, the HD signal in the low-temperature peak was found to be comparable to the D_2-only reference, providing no clear evidence that hydrogen transferred from the high-temperature to the low-temperature retention sites via isotope exchange. The current protocol was therefore not able to significantly reduce the population of the initially retained hydrogen isotope.

This wealth of new results on the interaction of hydrogen isotopes with boron calls for more systematic studies addressing the topics of hydrogen molecular dissociation on implanted boron, the chemical activity evolution of boron with thermal cycling, and the development of isotope exchange protocols to address nuclear safety issues related to tritium retention. We stress that these results were obtained on a thermodynamically stable β-phase of boron. However, boron layers created in fusion reactors are structurally different, which may affect their reactivity with hydrogen isotopes. Comparison with boron thin films deposited *in situ* on W substrates with varying impurity content must be pursued in order to understand the impact of both boron morphology and impurity content on hydrogen retention and release.

CRediT authorship contribution statement

A. Afonin: Writing – original draft, Visualization, Validation, Investigation, Formal analysis, Data curation. **T. Cornelius:** Formal analysis. **C. Martin:** Writing – review & editing, Investigation. **M. Minissale:** Writing – review & editing, Investigation, Formal analysis. **C. Pardanaud:** Writing – review & editing, Investigation, Data curation. **P. Rial Plaza:** Investigation. **E. Salomon:** Writing – review & editing, Investigation, Data curation. **T. Angot:** Writing – review & editing, Supervision, Project administration. **R. Bisson:** Writing – review & editing, Supervision, Project administration, Funding acquisition.

Declaration of competing interest

The authors declare that they have no known competing financial interests or personal relationships that could have appeared to influence the work reported in this paper.

Acknowledgments

This work has been carried out within the framework of the EUROfusion Consortium, funded by the European Union via the Euratom

Research and Training Programme (Grant Agreement No 101052200 - EUROfusion). Views and opinions expressed are however those of the author(s) only and do not necessarily reflect those of the European Union or the European Commission. Neither the European Union nor the European Commission can be held responsible for them. The work has been also carried out within the framework of the French Federation for Magnetic Fusion Studies (FR-FCM).

References

[1] J. Bucalossi, et al., Operating a full tungsten actively cooled tokamak: overview of WEST first phase of operation, Nucl. Fusion 62 (4) (2022) 042007.
[2] R.A. Causey, T.J. Venhaus, The use of tungsten in fusion reactors: A review of the hydrogen retention and migration properties, Phys. Scr. T94 (1) (2001) 9.
[3] P. Wang, et al., Hydrogen in mechanically milled amorphous boron, J. Alloys Compd. 350 (1–2) (2003) 218–221.
[4] P. Wang, et al., Characterization of hydrogenated amorphous boron by a combination of infrared absorption spectroscopy and thermal analyses, J. Alloys Compd. 359 (1–2) (2003) L1–L3.
[5] Y. Oya, et al., Implanted hydrogen isotope retention and chemical behavior in boron thin films for wall conditioning, J. Nucl. Mater. 329–333 (2004) 870–873.
[6] V. Alimov, et al., Deuterium retention in sintered boron carbide exposed to a deuterium plasma, J. Nucl. Mater. 349 (3) (2006) 282–290.
[7] Y. Yamauchi, et al., Hydrogen and helium retention properties of B4C and SiC converted graphites, Fusion Eng. Des. 39–40 (1998) 427–432.
[8] T. Hino, et al., Deuterium retention of boron–titanium and reduction of deuterium retention after helium ion irradiations, Fusion Eng. Des. 85 (5) (2010) 655–660.
[9] A. Hamada, et al., Study on the retention behavior of hydrogen isotopes and the change of chemical states of boron film exposed to hydrogen plasma in LHD, Fusion Eng. Des. 87 (7–8) (2012) 1214–1217.
[10] S. Abe, et al., Experimental setup to investigate hydrogen isotope retention on powder samples as slag/dust proxies for advanced fusion reactors, Fusion Sci. Technol. (2025) 1–10.
[11] H. Kodama, et al., Chemical behaviors of energetic deuterium implanted into boron coatings, Fusion Sci. Technol. 44 (2) (2003) 420–424.
[12] R. Pearce, L. Worth, ITER Vacuum Handbook, Technical Report ITR-19-004, ITER Organization, 2019.
[13] M. Minissale, et al., Sticking probability of ammonia molecules on tungsten and 316L stainless steel surfaces, J. Phys. Chem. C 124 (32) (2020) 17566–17577.
[14] P. Wagner, et al., Behavior of hydrogen ions, atoms, and molecules in α -boron studied using density functional calculations, Phys. Rev. B 83 (2) (2011) 024101.
[15] B. Mårlid, et al., Chemical Interaction of H_2 , Br_2 , and HBr with α -Boron Surfaces, J. Phys. Chem. B 105 (51) (2001) 12797–12802.
[16] T. Hiroto, et al., Lattice expansion due to hydrogen absorption into β -rhombohedral boron, Solid State Sci. 163 (2025) 107907.
[17] C. Louis De Canonville, et al., Optical properties, surface composition and desorption of stainless steel (316L) studied from ambient temperature to 1000 K in vacuum, Mater. Today Commun. 36 (2023) 106865.
[18] R. Bisson, et al., Dynamic fuel retention in tokamak wall materials: An in situ laboratory study of deuterium release from polycrystalline tungsten at room temperature, J. Nucl. Mater. 467 (2015) 432–438.
[19] M. Ialovega, et al., Deuterium retention in tungsten oxide: the role of oxide damage, Nucl. Fusion 65 (7) (2025) 076024, Publisher: IOP Publishing.
[20] F. Ghiorghiu, et al., Nitrogen retention and ammonia production on tungsten, Nucl. Fusion 61 (12) (2021) 126067.
[21] T. Aissou, et al., Deuterium retention and ammonia production from D-implanted 316 L stainless steel: insights for future fusion reactors, Mater. Res. Express 11 (2) (2024) 026510.
[22] G. Slack, et al., The crystal structure and density of β -rhombohedral boron, J. Solid State Chem. 76 (1) (1988) 52–63.
[23] G. Parakhonskiy, et al., Experimental pressure-temperature phase diagram of boron: resolving the long-standing enigma, Sci. Rep. 1 (1) (2011) 96.
[24] J. Qin, et al., Phase relations in boron at pressures up to 18 GPa and temperatures up to 2200 °C, Phys. Rev. B 85 (1) (2012) 014107.
[25] H. Werheit, et al., Isotopic phonon effects in β -rhombohedral boron—non-statistical isotope distribution, J. Phys.: Condens. Matter. 24 (17) (2012) 175401.
[26] J. Yeh, I. Lindau, Atomic subshell photoionization cross sections and asymmetry parameters: $1 \leq Z \leq 103$, At. Data Nucl. Data Tables 32 (1) (1985) 1–155.
[27] J. Yeh, Atomic Calculation of Photoionization Cross-Sections and Asymmetry Parameters, Gordon & Breach Science, Publishers, 1993.
[28] R. Basner, et al., Absolute total and partial cross sections for the electron impact ionization of diborane (B2H6), J. Chem. Phys. 118 (5) (2003) 2153–2158.
[29] A. Dunand, et al., Surface oxygen versus native oxide on tungsten: contrasting effects on deuterium retention and release, Nucl. Fusion 62 (5) (2022) 054002.